Published in final edited form as:
Radiat Res. 2013 August ; 180(2): 205–215. doi:10.1667/RR3237.1.

Quercetin Inhibits Radiation-Induced Skin Fibrosis

Jason A. Horton[a], **Fei Li**[b], **Eun Joo Chung**[a], **Kathryn Hudak**[a], **Ayla White**[a], **Kristopher Krausz**[b], **Frank Gonzalez**[b], and **Deborah Citrin**[a,1]

[a]Radiation Oncology Branch, National Cancer Institute, Bethesda, Maryland 20892

[b]Laboratory of Metabolism, National Cancer Institute, Bethesda, Maryland 20892

Abstract

Radiation induced fibrosis of the skin is a late toxicity that may result in loss of function due to reduced range of motion and pain. The current study sought to determine if oral delivery of quercetin mitigates radiation-induced cutaneous injury. Female C3H/HeN mice were fed control chow or quercetin-formulated chow (1% by weight). The right hind leg was exposed to 35 Gy of X rays and the mice were followed serially to assess acute toxicity and hind leg extension. Tissue samples were collected for assessment of soluble collagen and tissue cytokines. Human and murine fibroblasts were subjected to clonogenic assays to determine the effects of quercetin on radiation response. Contractility of fibroblasts was assessed with a collagen contraction assay in the presence or absence of quercetin and transforming growth factor-β (TGF-β). Western blotting of proteins involved in fibroblast contractility and TGF-β signaling were performed. Quercetin treatment significantly reduced hind limb contracture, collagen accumulation and expression of TGF-β in irradiated skin. Quercetin had no effect on the radioresponse of fibroblasts or murine tumors, but was capable of reducing the contractility of fibroblasts in response to TGF-β, an effect that correlated with partial stabilization of phosphorylated cofilin. Quercetin is capable of mitigating radiation induced skin fibrosis and should be further explored as a therapy for radiation fibrosis.

INTRODUCTION

Ionizing radiation is commonly used as a therapy for cancer, but can result in both acute and chronic damage to the skin. Radiation dermatitis is an acute radiation injury of the skin characterized by reversible erythema, pigment changes and desquamation (1). Acute radiation injury of the skin frequently resolves, whereas late radiation injury is characterized by loss of skin appendages, atrophy and an irreversible progressive fibrosis (2). Changes associated with late radiation injury of the skin may result in functional impairment and poor cosmesis. Identification of agents that can prevent or mitigate radiation damage is critical to reducing the morbidity of cutaneous radiation injury.

[1]Address for correspondence: Radiation Oncology Branch, CCR, National Cancer Institute, 10-CRC-Hatfield Clinical Research Center, B2-3500, Bethesda, MD 20892-1682; citrind@mail.nih.gov..

Editor's note. The online version of this article (DOI: 10.1667/RR3237.1) contains supplementary information that is available to all authorized users.

Quercetin is a plant-derived flavonol found in a variety of fruits and vegetables, with particularly high concentrations found in the outer skin of onions and shallots. Quercetin and its derivatives have been shown to inhibit inflammation and scarring in models of foreign-body reaction, hypertrophic scar formation and keloid (3, 4). Quercetin has been reported to reduce tumor necrosis factor-α and TGF-β expression, increase matrix metalloproteinase-1 activity and reduce oxidative stress (5, 6). As each of these mechanisms has been implicated in the development of radiation-induced fibrosis, we reasoned that quercetin would favorably modify the progression of this late toxicity. The purpose of this study was to evaluate the antifibrotic potential of quercetin in a small animal model of radiation induced dermal fibrosis. We hypothesized that oral delivery of quercetin would reduce the dermal fibrotic response to irradiation.

METHODS AND MATERIALS

Reagents

Quercetin hydrate [2-(3,4-dihydroxyphenyl)-3,5,7-trihydroxy-4H-1-benzopyran-4 one, 3,3′, 4′,5,6-pentahydroxyflavone] was obtained from Sigma Aldrich (St. Louis, MO). For *in vitro* studies, quercetin was reconstituted in DMSO immediately prior to use. For *in vitro* experiments, recombinant mouse TGF-β1 was obtained from Invitrogen/Life Technologies (Grand Island, NY) and activated as recommended by the manufacturer.

Leg Contracture Studies

All animal experiments were institutionally approved and deemed in accordance with the guidelines of the Institute of Laboratory Animal Resources, National Research Council. Female C3H/HeN mice, aged 8–10 weeks were used for leg contracture studies. Mice received rodent chow formulated with 1% quercetin by dry weight (Bio-Serv, Frenchtown, NJ) or identical chow without quercetin beginning one week prior to irradiation and continued for the duration of animal studies. Both groups were allowed *ad libitum* access to food and water. Body weight was evaluated weekly.

During irradiation, mice were immobilized in a Lucite jig that facilitated irradiation of the right hind leg while the remainder of the animal was protected by lead shields. A dose of 35 Gy was delivered to the right hind leg with a Pantak XRAD320 X-ray irradiator (Precision X-ray, Inc., East Haven, CT) using 2.0 mm Al filtration (300 kv peak) at a dose of 1.9 Gy/min. A published phenotypic scoring scale was used to evaluate early skin toxicity three times weekly during the first 11 weeks after irradiation (7). Briefly, a score of 1 = normal, 2 = alopecia, 3 = erythema, 4 = dry desquamation, 5 = <30% moist desquamation and 6 = >30% moist desquamation.

Hind leg contraction was evaluated in 8 mice per treatment group using a custom jig to facilitate measurement of hind leg extension with an accuracy of ±0.5 mm. The degree of contraction was measured by comparing the extension of the irradiated leg to that of the contralateral unirradiated leg at monthly intervals between 90 and 150 days after irradiation.

Additional mice were treated as described above and three mice per group per time point were euthanized at intervals after irradiation to provide tissues for histological and

biochemical analyses. Full-thickness skin tissue was sampled from the irradiated field, or an analogous site on the contralateral limb. Skin samples were snap frozen and stored at −80°C for biochemical assay or fixed in 10% neutral buffered formalin for histologic analysis.

Assessment of Quercetin Metabolism

Ten mice were treated with control or quercetin chow for one week for the purpose of evaluation of quercetin metabolism. Mice were allowed free access to chow, and weight and chow consumption were monitored daily. Urine was collected just prior to euthanasia. Blood was collected by cardiac puncture into heparinized syringes, immediately centrifuged at 4°C to produce plasma, aliquoted and snap frozen. The entire liver was collected. All samples were stored at −80°C until analysis.

To prepare urine 20 μL samples were mixed with 180 μL 50% aqueous acetonitrile and centrifuged at 18,000g for 20 min at 4°C. To prepare plasma, 200 μL samples were mixed with 1.0 mL 100% methanol and centrifuged at 18,000*g* for 20 min at 4°C. Samples of liver (300 mg) were minced in 1.0 ml 100% methanol, shaken for 15 min at room temperature and centrifuged at 18,000*g* for 20 min at 4°C. Supernatants from the urine, plasma and liver preparations were then dried in N_2 and dissolved in 200 μL 67% aqueous acetonitrile.

UPLC-ESI-QTOFMS and Multivariate Data Analysis

A 5 μL aliquot of the prepared sample was chromatographed by ultra-performance liquid chromatography (Waters Corp, Milford, MA) using a 2.1 × 50 mm Waters BEH C18 1.7 μm column and introduced by electrospray into a quadrupole time-of-flight mass spectrometer (UPLC-ESI-QTOFMS). The gradient mobile phase consisted of 0.1% formic acid solution (A) and acetonitrile containing 0.1% formic acid solution (B). The gradient was maintained at 100% (A) for 0.5 min, increased to 100% (B) over the next 7.5 min and returning to 100% (A) in the last 2 min. Data were collected in positive and negative mode, which was operated in full-scan mode from 100 to 1,000 *m/z*. Nitrogen was used as both cone gas (50 liters/h) and desolvation gas (600 liters/h). Source and desolvation temperature were set at 120 and 350°C, respectively. The capillary and cone voltage were 3,000V and 20V, respectively. Chlorpropamide (5 μ*M*) was added in the sample as the internal standard. Raw data from the UPLC-ESI-QTOFMS system were aligned using MarkerLynx software (Waters) to generate a data matrix consisting of peak areas corresponding to a unique *m/z* and retention time. The generated multivariate data matrix was exported into SIMCA-P +12.0 (Umetrics, Kinnelon, NJ) for principal component analysis (PCA) and partial least-squares discriminant analysis (PLS-DA). The quercetin metabolites were initially determined by analyzing the ions in the loadings scatter plot. The identity of metabolites was determined by their mass fragmentation as previously described (8–10).

Histology

To evaluate tissue architecture, 6 μm thick paraffin embedded tissue sections were stained by Masson’s trichrome technique (Sigma) and examined by light microscopy. Digital images were captured at 10× magnification using a Photometrics Sensys CCD camera (Roper Scientific, Tucson, AZ) and processed using Image J software (National Institutes of Health, Bethesda, MD).

Assessment of TGF-β Expression and Collagen Accumulation

For determination of total TGF-β, skin tissue was homogenized in ice-cold RIPA buffer containing protease and phosphatase inhibitors (10 ml/g tissue, Thermo Scientific, IL). After centrifugation, the concentration of total soluble TGF-β in the supernatant was measured using a sandwich ELISA assay (R&D Systems, Minneapolis, MN) in accordance with the manufacturer's recommended protocol. The concentration of total TGF-β was calculated by interpolation to a standard curve of known TGF-β concentrations and normalized by tissue weight.

A colorimetric dye-binding assay was used to assess the accumulation of fibrillar collagen in skin samples as previously described (11). Briefly, skin samples were minced and digested overnight in 0.5% pepsin/0.5 *M* acetic acid at 37°C with vigorous shaking. After centrifugation, supernatants were mixed with equal volumes of 0.1% Sirius Red dye in saturated picric acid (Electron Microscopy Sciences, Hatfield, PA). Collagen-dye complexes were pelleted by centrifugation, washed with 0.5 *M* acetic acid, and solubilized with 0.5 *M* sodium hydroxide. Absorbance of the released dye (562 nm) was read on a microplate reader, converted to collagen equivalents by interpolation to a standard curve of known concentrations of rat type I collagen (Sigma) and normalized to tissue weight.

Cells and Collagen Gel Contraction Assay

The NIH-3T3 and BJ cell lines were obtained from ATCC (Manassas, VA). NIH-3T3 cells were cultured in DMEM (Invitrogen) supplemented with 10% fetal calf serum (FCS, Gemini Bioproducts, West Sacramento, CA). BJ cells were cultured in RPMI (Quality Biological, Gaithersburg, MA) with 10% FCS. The HEKblue-TGF-β reporter cell line (InvivoGen, San Diego, CA) was maintained in DMEM media with 10% FCS and the manufacturers recommended cocktail of selection antibiotics. Cells were maintained in an exponential growth phase at 37°C, 5% CO_2.

Fibroblast contractility was assessed by the collagen gel contraction assay described previously (12). Briefly, NIH-3T3 cells were suspended (2×10^5 cells/ml) in a neutralized 1 mg/ml solution of type I collagen (Invitrogen), transferred in 0.5 ml aliquots to 24-well tissue culture plates, and incubated for 30 min at 37°C to solidify. Once solidified, gels were released from the wall of the tissue culture plate using a sterile inoculating loop and allowed to float freely in 1 ml of media containing 1 μ*M* quercetin or 0.1% DMSO vehicle. One hour later, recombinant TGF-β (5 ng/mL final concentration) was added. The average diameter of the gels was measured at 24 h and normalized to the contraction of gels receiving only DMSO vehicle without TGF-β. All data are derived from three replicate experiments with four gels assessed per independent experiment.

Western Blotting and Co-immunoprecipitation Assays

Western blotting was performed to assess expression and phosphorylation status of cytoskeletal regulatory proteins. Briefly, NIH-3T3 cells at ~70% confluence were preconditioned for 16 h in DMEM with 1% FCS. Thereafter, cells were washed and incubated with DMEM/1% FCS containing 1 μ*M* quercetin, or 0.1% DMSO vehicle. After 1 h, recombinant TGF-β was added at a final concentration of 5 ng/ml. Cell lysates were

prepared in RIPA buffer containing protease and phosphatase inhibitors. Equal amounts of protein were resolved by SDS-PAGE and transferred to nitrocelulose membranes. After washing and blocking, membranes were incubated with primary antibodies followed by horseradish-peroxidase-conjugated secondary antibodies (see Supplementary Material Table 1S; http://dx.doi.org/10.1667/RR3237.1.S1) and visualized by chemiluminescence. Glyceraldehyde-3-dehydrogenase (GAPDH) was probed as a loading control.

Co-immunoprecipitation experiments were performed to evaluate the effects of quercetin on TGF-β induced SMAD3/4 complex formation in NIH 3T3 cells. Cells were treated as described for Western blotting, lysed in a nondenaturing buffer (1% NP-40, 10 m*M* Tris pH7.8, 150 m*M* NaCl) supplemented with protease and phosphatase inhibitors. Lysates were clarified by centrifugation and supernatants containing 1 mg total protein were reacted with 2 μg of a mouse anti-SMAD4 antibody (Santa Cruz Biotechnologies, Santa Cruz, CA). Immune complexes were then precipitated on protein A-Agarose beads (Upstate/Millipore, Billerca, MA), released by boiling in reducing sample buffer and subjected to Western blotting with rabbit antibodies to phospho-SMAD3 and SMAD4. Whole cell lysates were also subjected to Western blotting to demonstrate consistency of expression prior to immunoprecipitation.

TGF-β Inducible Reporter Assay

We used a HEK293 cell-based reporter assay system to determine whether quercetin altered the transcriptional regulation of TGF-β target genes. This reporter cell expresses secreted embryonic alkaline phosphatase downstream from a promoter containing 3 copies of the SMAD3/4 binding element. Cells were incubated with 1 μ*M* quercetin or 0.1% DMSO for 1 h prior to addition of 5 ng/ml TGF-β1 or PBS vehicle and incubated for an additional 16 h. Supernatants from the reporter cells were clarified by centrifugation, added to QUANTI-Blue™ alkaline phosphatase detection media (InvivoGen) and incubated at 37°C for 3 h. Reporter activity was calculated as the relative increase in absorbance at 620 nm between media of vehicle/DMSO treated cells and the combination of DMSO/TGF-β or quercetin and TGF-β. Data from these reporter experiments are the average ±SEM of three independent experiments.

Immunocytochemistry

NIH-3T3 cells were plated on collagen-coated glass chamber slides. At 50% confluence, the cells were washed with PBS and incubated in media containing 1 μ*M* quercetin and/or 5 ng/ml TGF-β or 0.1% DMSO vehicle. After 30 min (Smad4/phospho-Smad3) or 24 h (phospho-Cofilin/Actin), the cells were washed with ice cold PBS, fixed for 10 min in 2% paraformaldehyde in PBS, quenched for 10 min with 0.3 *M* glycine in PBS and permeabilized with 0.1% Triton-X100. The cells were blocked with 1% BSA in PBS, followed by incubation for 1 h with antibodies against phospho-cofilin (Cell Signaling Technologies), phosphoSMAD3 (Epitomics/AbCam) or Smad4 (Santa Cruz Biotechnology Inc.). Immunoreactivity was visualized by incubating for 1 h with an Alexafluor-488 or Alexafluor-594 conjugated secondary antibody diluted in blocking buffer. Actin cytoskeleton was stained by incubating with 50 nM TRIT-C Phalloidin (Sigma) for 15 min. Cell nuclei were stained 10 ng/ml DAPI (Sigma) for 10 min in PBS and cover slipped with

ProLong Gold antifade media (Invitrogen). Epifluorescent images were digitally captured at 63× magnification and merged with Image J software (NIH) for qualitative assessment of cytoskeletal morphology and localization of phospho-cofilin, phospho-Smad3 and Smad4.

Clonogenic Assay

NIH-3T3 and BJ cell cultures were trypsinized to generate a single cell suspension and were seeded into six-well tissue culture plates. After allowing 5 h for attachment, the cells were incubated with quercetin or DMSO (vehicle control) for 1 h prior to and 24 h after irradiation. Cultures were irradiated with 2 Gy using a Pantak (Solon, OH) X-ray source at a dose rate of 1.55 Gy/min. Ten days after seeding, colonies were stained with crystal violet, the number of colonies containing at least 50 cells was determined and the surviving fractions were calculated. Survival curves were generated after normalizing for cytotoxicity generated by quercetin alone. Data presented are the mean ± SEM from at least three independent experiments.

Tumor Model

Subcutaneous tumors were initiated by inoculating 2.5×10^5 cell syngeneic squamous cell carcinoma cells (SCC-VII provided by James B. Mitchell, NIH, validated at RADIL) into the right hind leg of eight-week-old female C3H/HeN mice. Tumor growth was measured every three days and volumes were calculated using a formula $(l \times w \times w)/2$. Pilot studies showed that delivery of quercetin chow for greater than 24 h to tumor bearing mice resulted in tumor growth inhibition. As tumor size at the time of irradiation is known to alter radiation response (13, 14) mice were treated with quercetin chow in subsequent experiments only during the 24 h immediately prior to and after irradiation. When tumors grew to a mean volume of 136 mm^3, the mice were randomized to control chow, quercetin chow, control chow + irradiation or quercetin chow + irradiation. Mice randomized to irradiation groups received a dose of 10 Gy to the tumor-bearing limbs as described above. Quercetin chow was discontinued 24 h after irradiation, and tumor growth was measured three times weekly until the mean tumor volume for each group reached 1,500 mm^3. Tumor growth delay was calculated for each animal. The mean delay was calculated as the number of days for the treated tumors to grow to 1,500 mm^3 minus the number of days for the control group to reach the same size. Each experimental group contained at least seven mice.

Statistical Analyses

In vitro experiments were conducted in three independent experiments and statistical analysis was done using Student's *t* test. A probability level of $P < 0.05$ was considered significant. *In vivo* experiments were performed in duplicate and presented as mean ± standard error. Tissue assays were performed in triplicate on at least 3 samples per condition per time point.

RESULTS

Quercetin Decreases Radiation-Induced Hind Limb Contracture and Dermal Thickening

Dermal fibrosis with resultant contracture is a reproducible event in the murine model of cutaneous radiation-induced fibrosis. Extension of the irradiated hind limb was measured at

90, 120 and 150 days after irradiation. All mice showed progressive contracture of the irradiated hind limb, however this was significantly reduced in quercetin-treated mice at 120 and 150 days (Fig. 1A, $P \leq 0.05$) compared to control chow-fed mice.

Histologically, irradiated skin exhibited extensive dermal collagen accumulation, epithelial thickening and hyperkeratosis (Fig. 1B). Quercetin-treated mice exhibited a reduction of these changes. Additionally, skin appendages such as hair follicles and glands were not observed in the irradiated skin of control mice, but were preserved in the irradiated skin of quercetin-treated mice.

Tolerance to Therapy

No significant differences were observed in chow consumption (data not shown) and body weight (Fig. 1C) between control chow and quercetin-treated mice. There was no significant difference in the onset, severity or duration of acute irradiation skin reaction in groups of mice treated with quercetin chow or control chow (Fig. 1D).

Quercetin Reduces Collagen Accumulation and TGF-β Levels in Irradiated Skin

Collagen accumulation was greater in the irradiated skin, relative to the contralateral side at all time points ($P < 0.05$, Fig. 2A). The irradiated skin of quercetin-treated mice showed significantly reduced collagen levels at 120 and 150 days compared to control chow-fed mice ($P \leq 0.0035$). There were no significant differences in collagen content in unirradiated skin between control and quercetin treated mice.

Quercetin treatment significantly reduced TGF-β levels in the irradiated skin ($P \leq 0.05$) in comparison to irradiated control tissues at 60 and 150 days (Fig. 2B). Although reduced compared to control fed mice, TGF-β remained elevated in quercetin-fed irradiated samples compared to unirradiated samples. No significant differences in TGF-β levels of unirradiated skin were observed between control and quercetin treated mice.

Quercetin Decreases the Contractility of Fibroblasts

Quercetin treatment reduced contractility of fibroblasts suspended in a collagen gel in response to treatment with TGF-β (Fig. 3A). Gels incubated with TGF-β alone contracted to a diameter 71.9% ($P \leq 0.0001$) that of untreated controls. In contrast, no significant difference in contraction was measured in gels treated with quercetin alone (101.8%, $P = 0.6559$) or in combination with TGF-β (93.6% $P = 0.0969$). Densitometric analysis of Western blots revealed that TGF-β strongly reduced cofilin phosphorylation. Quercetin treated cells showed slightly increased cofilin phosphorylation compared to vehicle treated controls (Fig. 3B). When combined with TGF-β, quercetin restored phospho-cofilin to near control levels at 24 h of treatment. Qualitatively, immunocytochemistry also showed marked reduction of phospho-cofilin in TGF-β treated fibroblasts, which was largely abrogated by quercetin treatment. Most notably, fibroblasts incubated with TGF-β displayed prominent actin-stress fibers and filopodial extensions that were greatly reduced by co-treatment with quercetin (Fig. 3C). Several proteins involved with regulating cofilin activity were also examined, including ROCK, PDXP/CIN and phosphorylated LimK1/2 (Fig. 3B) as reviewed by Oser and Condeelis (15), but did not appear to be affected by quercetin treatment.

Furthermore, heme oxygenase-1, phospho-smad3 and phospho-c-Abl were not altered with quercetin treatment and TGF-β stimulation compared to that observed with TGF-β alone.

We then sought to determine whether quercetin disrupted signaling downstream of TGF-β. In co-immunoprecipitation and immunofluorescence experiments, quercetin did not alter TGF-β-induced Smad3/4 complex formation or nuclear translocation (Fig. 4A and B). Similarly, quercetin did not significantly alter the TGF-β-induced activity of a Smad3/4 transcriptional reporter (Fig. 4C). Taken together, these data suggest that quercetin may elicit its antifibrotic effect by inhibiting fibroblast contractility in a cofilin-dependent manner, rather than a direct effect on TGF-β-induced signal transduction and Smad3/4 mediated gene expression.

Quercetin did not Protect Fibroblasts or Tumors from Irradiation

Previously, it was suggested that quercetin may alter the radioresponse of human tumor cell lines and xenografts (16). The ability of quercetin to provide a direct radioprotective benefit to nonmalignant cells was examined *in vitro* using clonogenic survival assays. No radioprotective benefit was observed at the doses tested (1 to 10 μ*M*) in either human or murine fibroblast cell lines (Fig. 5A). This suggests that the antifibrotic effect of quercetin was not a result of radioprotection of the cells in normal tissues.

The radioprotective potential of quercetin was also tested in the context of an *in vivo* tumor-irradiation model. Tumors were treated at a volume of 136 ± 16 mm^3 and were followed until they exceeded 1,500 mm^3 (Fig. 5B). Without irradiation, the time required to exceed 1,500 mm^3 was not significantly different between mice fed quercetin (7.25 ± 0.4 days) or control chow (6.6 ± 0.7 days). Similarly, the treatment of quercetin + 10 Gy did not significantly alter the time required to exceed 1,500 mm^3 (10.3 ± 2.6 days) compared to control chow-fed + 10 Gy (11.9 ± 1.4). Absolute growth delays (corrected for the time for unirradiated controls to reach 1,500 mm^3) were 0.63 days for quercetin alone, 5.2 days for irradiation alone and 3.7 days for quercetin + 10 Gy. These data suggest that there was no alteration of tumor sensitivity to irradiation associated with dietary quercetin treatment

Quercetin Metabolites are Evident after Oral Administration

Quercetin is extensively metabolized through glucuronation, sulfation and/or methylation. The predominant metabolites in the plasma, liver and urine were examined in mice fed quercetin chow at the dose shown to have antifibrotic efficacy. The consumption of control chow and quercetin chow (1.17 vs. 1.02 gm, $P = 0.55$) and weight gain (160 vs. 155 gm/week, $P = 0.82$) in the two groups was similar.

Metabolomics analysis revealed significant differences in urine and plasma between the quercetin group and control group (Fig. 6A and B). An S plot showed that the metabolites contributing to the separation of both groups were derived from quercetin, which were initially determined by the trending plot of the ion (see Supplementary Material Fig. S1A and B; http://dx.doi.org/10.1667/RR3237.1.S2). The identity of metabolites was determined through their mass fragmentation patterns (see Supplementary Material Fig. S1C and D; http://dx.doi.org/10.1667/RR3237.1.S2). A number of metabolites were detected in urine,

plasma and liver homogenate after quercetin chow feeding for one week, including methylated and glucuronated derivatives (Fig. 6C–E). Only three metabolites were readily evident in plasma, quercetin diglucuronide, methylquercetin sulfate and methylquercetin diglucuronide (Fig. 6C). Six metabolites were observed in liver including quercetin diglucuronide, methylquercetin diglucuronide, quercetin glucuronide and methylquercetin glucuronide (Fig. 6D). From these data, the only metabolite found in high abundance in the liver, plasma and urine was quercetin diglucuronide. All metabolites identified in urine, plasma and liver are summarized in Table 1.

DISCUSSION

Oral delivery of quercetin is sufficient to reduce hind leg contraction in a murine model of cutaneous radiation-induced fibrosis. Reduced contracture was associated with a reduction in collagen content and TGF-β elaboration in irradiated skin. Quercetin treatment was well tolerated and did not influence the severity of acute radiation dermatitis.

The model used in this study is a well-accepted model of cutaneous radiation fibrosis (17–19) that uses a single fraction of 35 Gy. Delivery of large fractional doses of radiation is becoming more widespread due to the proliferation of stereotactic procedures in clinical practice. Furthermore, this model approximates the injury that could be expected from an accidental exposure.

Direct radioprotection is one possible explanation for the ability of quercetin to reduce cutaneous fibrosis. Quercetin has been shown to prevent DNA damage via antioxidant mechanisms (20). Similarly, Musonda *et al.* (21) demonstrated reduction of oxygen radical-induced DNA strand breakage and DNA binding by NF-κB in quercetin treated HepG2 cells. A single study evaluated the ability of quercetin to protect against total body irradiation (TBI) exposures in mice (22). Although quercetin pretreatment increased leukocyte counts after TBI, a benefit was also observed with post-TBI delivery of quercetin, a finding inconsistent with classical radioprotection. Furthermore, the relevance of this degree of leukocyte protection is unclear, as survival was not measured as an endpoint. This current study documented a lack of clonogenic radioprotection from quercetin treatment in non-malignant tissues.

Lin *et al.* recently reported radiation enhancement with quercetin in human tumor cell lines and xenografts (16). However, at similar concentrations, no evidence of sensitization of mouse or human fibroblast cell lines was observed in the present study. Furthermore, the observed absence of increased toxicity in mice treated with both quercetin and radiation supports a lack of normal tissue radiosensitization. Importantly, we observed no evidence of radioprotection was observed in a murine carcinoma tumor model with oral delivery of quercetin. Exposure to quercetin-modified chow for longer than 24 h was observed to inhibit tumor growth, suggesting that quercetin was delivered to the tumor at effective doses, despite the absence radiation modification. One potential explanation for this difference in radiation modifying capacity is the mode of quercetin delivery (oral vs. intraperitoneal), which may result in different pharmacokinetic or pharmacodynamic effects. Quercetin was rapidly cleared from plasma after i.v. administration, with an estimated half-life of 20 min

(23). While the current study was not designed to determine these parameters, it was reasoned that dietary delivery of quercetin would generate a steady state level of the compound or its bioactive metabolites.

To that end, the presence of quercetin metabolites in liver and plasma of mice was confirmed using a metabolomics approach after delivery of quercetin chow at the dose that was effective in reducing fibrosis. Quercetin diglucuronide and methylquercetin sulfate were shown as high abundance in the plasma, while other phase II metabolites of quercetin with low abundance were not detected in plasma, such as quercetin glucuronide and quercetin sulfate (24, 25). Interestingly, quercetin diglucuronide was detected at high abundance in the liver, plasma and urine after quercetin treatment. Previous studies reported that various quercetin metabolites showed antioxidant activity, especially for quercetin 3-glucuronide and quercetin 3-O-sulfate (26). Additionally, quercetin glucuronides were reported to show inhibitory effects on human lung cancer and atherosclerotic arteries (27, 28). The current data demonstrate that oral administration yields a measurable level of metabolites in body fluids and tissues at doses that demonstrate antifibrotic efficacy. Furthermore, detection of these metabolites in accessible bodily fluids suggests that they may be useful markers of effective dosing. Taken together, these data identify quercetin diglucuronide and methylquercetin sulfate as attractive candidates for future studies in the setting of fibrosis.

Differentiation of tissue stromal fibroblasts toward the contractile myofibroblastic phenotype can be induced by elevated TGF-β and is a critical component of wound healing and fibrotic disorders (29, 30). Using a porcine model of late radiation-induced skin injury, Reisdorf *et al.* (31) demonstrated a differential expression of SMAD3 and SMAD2 and TGF-β-induced transcriptional activation when comparing normal dermal fibroblasts and myofibroblasts isolated from the irradiated dermis. Quercetin largely inhibited TGF-β-induced fibroblast contractility in a collagen gel contraction assay. Interestingly, this effect of quercetin was not due to direct alteration of TGF-β signal transduction, as Smad3 phosphorylation and heme-oxygenase-1 expression were not reduced. In a similar experiment, others (32) showed that several flavonoids, including quercetin, inhibit contraction of both primary and immortalized human dermal fibroblasts stimulated by endothelin-1(ET-1). That these stimuli are transduced by distinct signaling pathways suggested that quercetin might affect contractility or cytoskeletal organization at a downstream convergence point.

In the present study, fibroblasts treated with quercetin showed increased levels of the inactive, phosphorylated form of cofilin, despite no observed difference in the expression of total cofilin or its upstream regulatory proteins. Quercetin was also shown not to disrupt TGF-β-induced signal transduction and downstream activation of a Smad3/4 reporter. Immunocytochemical studies demonstrated that quercetin dramatically attenuates TGF-β-induced alterations of the actin cytoskeleton and restores the level and localization of cofilin. Bohl *et al.* observed a dose-dependent decrease of cofilin/gelsolin dependent actin polymerization in response to quercetin and other several other flavonoids (33). While their biophysical data suggest a direct interaction of several flavonoids with hydrophobic pocket in the structure of monomeric actin, their experiments did not examine what impact this interaction may have on the regulation of cofilin phosphorylation and therefore its activity.

Taken together, these data suggest that quercetin may elicit at least a portion of its antifibrotic effect by altering cytoskeletal organization and myofibroblast contractility in a manner that is not directly a consequence of a TGF-β-induced signaling mechanism.

In conclusion, the present study provides new evidence that quercetin may have a role in the management of radiation induced fibrosis. Coupled with previously published data reporting sensitization of tumor cells to irradiation with quercetin treatment, these data strongly support the further evaluation of quercetin and its bioactive metabolites, as a radiation mitigator.

Supplementary Material

Refer to Web version on PubMed Central for supplementary material.

ACKNOWLEDGMENTS

This research was supported by the Intramural Research Program of the NIH, NCI.

REFERENCES

1. Ryan JL. Ionizing radiation: The good, the bad, and the ugly. J Invest Dermatol. 132:985–93. [PubMed: 22217743]
2. Hall, EJ.; Giaccia, AJ. Radiobiology for the radiologist. 6th. Lippincott Williams & Wilkins; Philadelphia: 2006.
3. Rotelli AE, Guardia T, Juarez AO, de la Rocha NE, Pelzer LE. Comparative study of flavonoids in experimental models of inflammation. Pharmacol Res. 2003; 48:601–6. [PubMed: 14527825]
4. Phan TT, See P, Tran E, Nguyen TT, Chan SY, Lee ST, et al. Suppression of insulin-like growth factor signalling pathway and collagen expression in keloid-derived fibroblasts by quercetin: Its therapeutic potential use in the treatment and/or prevention of keloids. Br J Dermatol. 2003; 148:544–52. [PubMed: 12653748]
5. Wadsworth TL, Koop DR. Effects of the wine polyphenolics quercetin and resveratrol on pro-inflammatory cytokine expression in raw 264.7 macrophages. Biochem Pharmacol. 1999; 57:941–9. [PubMed: 10086329]
6. Phan TT, Lim IJ, Chan SY, Tan EK, Lee ST, Longaker MT. Suppression of transforming growth factor beta/smad signaling in keloid-derived fibroblasts by quercetin: Implications for the treatment of excessive scars. J Trauma. 2004; 57:1032–7. [PubMed: 15580028]
7. Randall K, Coggle JE. Expression of transforming growth factor-beta 1 in mouse skin during the acute phase of radiation damage. Int J Radiat Biol. 1995; 68:301–9. [PubMed: 7561390]
8. Li F, Patterson AD, Krausz KW, Dick B, Frey FJ, Gonzalez FJ, et al. Metabolomics reveals the metabolic map of procainamide in humans and mice. Biochem Pharmacol. 2012; 83:1435–44. [PubMed: 22387617]
9. Li F, Patterson AD, Hofer CC, Krausz KW, Gonzalez FJ, Idle JR. A comprehensive understanding of thiotepa metabolism in the mouse using uplc-esi-qtofms-based metabolomics. Biochem Pharmacol. 2011; 81:1043–53. [PubMed: 21300029]
10. Li F, Patterson AD, Hofer CC, Krausz KW, Gonzalez FJ, Idle JR. Comparative metabolism of cyclophosphamide and ifosfamide in the mouse using uplc-esi-qtofms-based metabolomics. Biochem Pharmacol. 2010; 80:1063–74. [PubMed: 20541539]
11. Lareu RR, Zeugolis DI, Abu-Rub M, Pandit A, Raghunath M. Essential modification of the sircol collagen assay for the accurate quantification of collagen content in complex protein solutions. Acta Biomater. 2011; 6:3146–51. [PubMed: 20144751]
12. Ngo P, Ramalingam P, Phillips JA, Furuta GT. Collagen gel contraction assay. Methods Mol Biol. 2006; 341:103–9. [PubMed: 16799192]

13. Suit HD, Walker AM. Assessment of the response of tumours to radiation. Br J Cancer Suppl. 1980; 4:1–10. [PubMed: 7000117]
14. Suit H, Schlachter L, Andrews JR. “Oxygen effect” and tumor size as related to response of c3h/ba adenocarcinoma to local x irradiation. J Natl Cancer Inst. 1960; 24:1271–81. [PubMed: 13835589]
15. Oser M, Condeelis J. The cofilin activity cycle in lamellipodia and invadopodia. J Cell Biochem. 2009; 108:1252–62. [PubMed: 19862699]
16. Lin C, Yu Y, Zhao HG, Yang A, Yan H, Cui Y. Combination of quercetin with radiotherapy enhances tumor radiosensitivity in vitro and in vivo. Radiother Oncol. 2012; 104:395–400. [PubMed: 22119371]
17. Molin J, Sogaard PE, Overgaard J. Experimental studies on the radiation-modifying effect of bleomycin in malignant and normal mouse tissue in vivo. Cancer Treat Rep. 1981; 65:583–9. [PubMed: 6166372]
18. Stone HB. Leg contracture in mice: An assay of normal tissue response. Int J Radiat Oncol Biol Phys. 1984; 10:1053–61. [PubMed: 6746346]
19. Xavier S, Piek E, Fujii M, Javelaud D, Mauviel A, Flanders KC, et al. Amelioration of radiation-induced fibrosis: Inhibition of transforming growth factor-beta signaling by halofuginone. J Biol Chem. 2004; 279:15167–76. [PubMed: 14732719]
20. Londhe JS, Devasagayam TP, Foo LY, Ghaskadbi SS. Radioprotective properties of polyphenols from phyllanthus amarus linn. J Radiat Res. 2009; 50:303–9. [PubMed: 19461166]
21. Musonda CA, Chipman JK. Quercetin inhibits hydrogen peroxide (h2o2)-induced nf-kappab DNA binding activity and DNA damage in hepg2 cells. Carcinogenesis. 1998; 19:1583–9. [PubMed: 9771928]
22. Benkovic V, Knezevic AH, Dikic D, Lisicic D, Orsolic N, Basic I, et al. Radioprotective effects of quercetin and ethanolic extract of propolis in gamma-irradiated mice. Arh Hig Rada Toksikol. 2009; 60:129–38. [PubMed: 19581205]
23. Ferrer P, Asensi M, Segarra R, Ortega A, Benlloch M, Obrador E, et al. Association between pterostilbene and quercetin inhibits metastatic activity of b16 melanoma. Neoplasia. 2005; 7:37–47. [PubMed: 15736313]
24. Rupasinghe HP, Ronalds CM, Rathgeber B, Robinson RA. Absorption and tissue distribution of dietary quercetin and quercetin glycosides of apple skin in broiler chickens. J Sci Food Agric. 90:1172–8. [PubMed: 20393998]
25. Mullen W, Edwards CA, Crozier A. Absorption, excretion and metabolite profiling of methyl-, glucuronyl-, glucosyl- and sulphoconjugates of quercetin in human plasma and urine after ingestion of onions. Br J Nutr. 2006; 96:107–16. [PubMed: 16869998]
26. Williamson G, Barron D, Shimoi K, Terao J. In vitro biological properties of flavonoid conjugates found in vivo. Free Radic Res. 2005; 39:457–69. [PubMed: 16036321]
27. Kawai Y, Nishikawa T, Shiba Y, Saito S, Murota K, Shibata N, et al. Macrophage as a target of quercetin glucuronides in human atherosclerotic arteries: Implication in the anti-atherosclerotic mechanism of dietary flavonoids. J Biol Chem. 2008; 283:9424–34. [PubMed: 18199750]
28. Yang JH, Hsia TC, Kuo HM, Chao PD, Chou CC, Wei YH, et al. Inhibition of lung cancer cell growth by quercetin glucuronides via g2/m arrest and induction of apoptosis. Drug Metab Dispos. 2006; 34:296–304. [PubMed: 16280456]
29. Moulin V, Auger FA, Garrel D, Germain L. Role of wound healing myofibroblasts on re-epithelialization of human skin. Burns. 2000; 26:3–12. [PubMed: 10630313]
30. Sarrazy V, Billet F, Micallef L, Coulomb B, Desmouliere A. Mechanisms of pathological scarring: Role of myofibroblasts and current developments. Wound Repair Regen. 19(Suppl 1):s10–5. [PubMed: 21793960]
31. Reisdorf P, Lawrence DA, Sivan V, Klising E, Martin MT. Alteration of transforming growth factor-beta1 response involves down-regulation of smad3 signaling in myofibroblasts from skin fibrosis. Am J Pathol. 2001; 159:263–72. [PubMed: 11438473]
32. Jun JB, Na YI, Kim TH, Yoo DH. Dietary flavonoid apigenin inhibits endothelin-1-induced contraction of collagen gel. Rheumatol Int. 30:1695–7. [PubMed: 20012048]
33. Bohl M, Tietze S, Sokoll A, Madathil S, Pfennig F, Apostolakis J, et al. Flavonoids affect actin functions in cytoplasm and nucleus. Biophys J. 2007; 93:2767–80. [PubMed: 17573428]

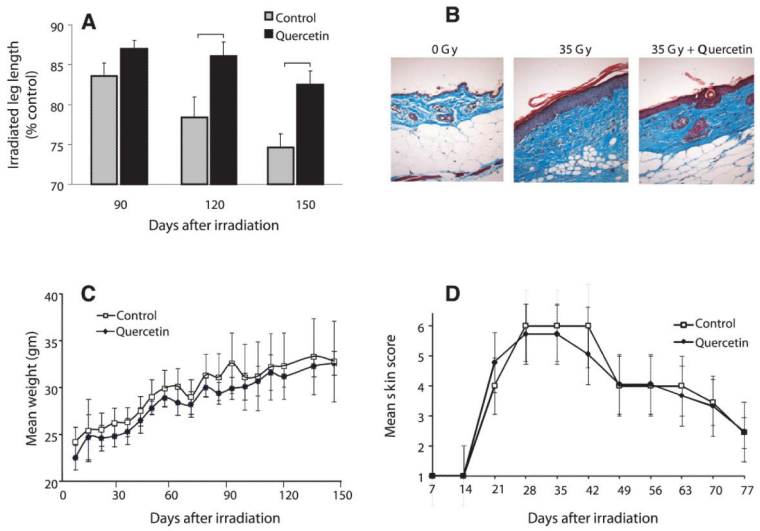

FIG. 1.

Quercetin reduces hind leg contraction after irradiation. Panel A: Serial assessment of hind limb contracture after irradiation. Data shown are mean percentage contracture ± SEM; brackets: $P < 0.05$, n = 8 per group. Panel B: Representative Masson trichrome staining at 150 days postirradiation, 10× magnification (collagen = blue, muscle/epithelial layers = red). Panel C: Body weight was not significantly affected by quercetin treatment. Data shown are mean body weight ± SEM. Panel D: Acute skin toxicity was unchanged by quercetin treatment. Data shown are mean score ± SEM.

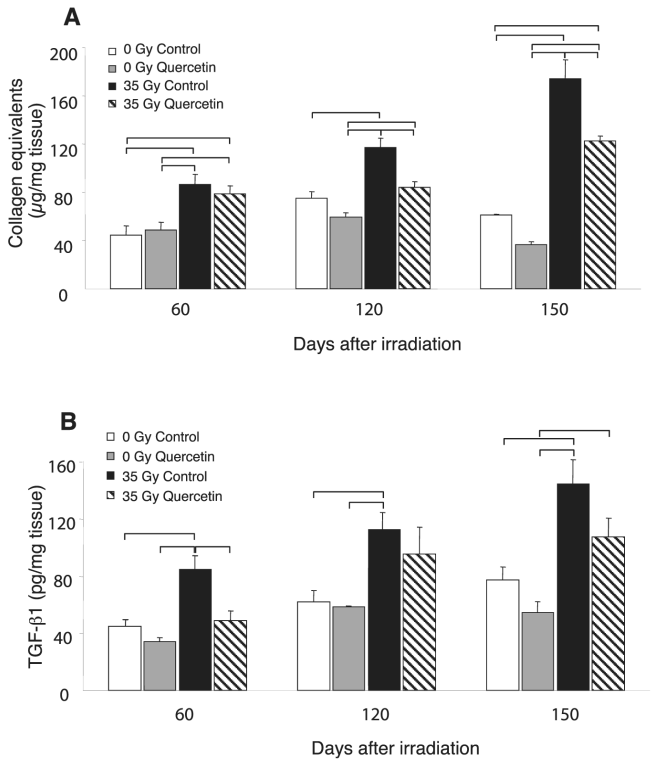

FIG. 2.

Quercetin alters collagen accumulation and TGF-β levels. Panel A: Sirius red binding assay was used to determine concentrations of acid-pepsin soluble collagen in skin samples. Data shown are mean normalized collagen content ±SEM; brackets: $P \leq 0.05$. Panel B: Levels of total TGF-β in homogenates of skin tissue were determined by ELISA. Data shown are mean TGF-β content ± SEM; brackets: $P \leq 0.05$. For both assays, sample values were interpolated from a standard curve and normalized to tissue weight.

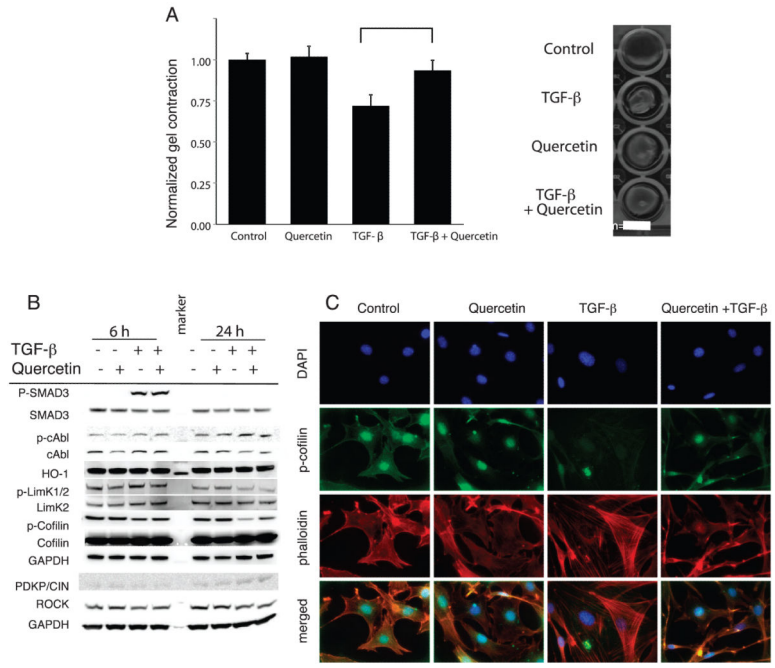

FIG. 3.

The effects of quercetin on fibroblast contractility. Panel A: Collagen gel contraction assay was used to assess contractility of fibroblasts following incubation with 5 ng/ml TGF-β and/or 1 μ*M* quercetin. Data shown are mean gel diameter ± SEM (left panel) and representative gels (right panel). Panel B: Western blotting demonstrates that quercetin does not disrupt signaling through TGF-β/SMAD or c-Abl pathways in NIH-3T3 cells, but instead affects cytoskeletal organization mediated by cofilin. Panel C: Immunocytochemistry demonstrated that quercetin reduced sensitivity of NIH/3T3 fibroblasts to TGF-β-induced stress fiber formation. Representative images showing localization of nuclei (blue = DAPI) phospho-cofilin (green = AF488) and actin (red = TRIT-C phalloidin) at 63× magnification.

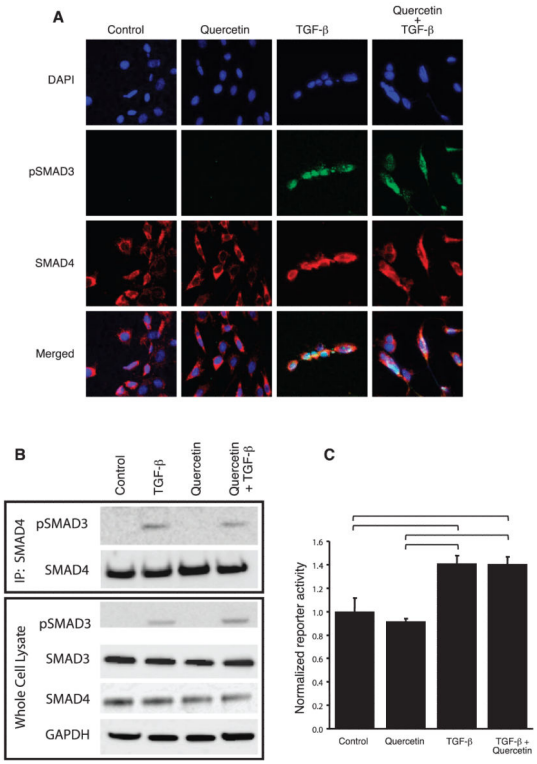

FIG. 4.

Effects of quercetin on Smad3/4 complex formation and TGFβ-induced gene expression. Panel A: Co-immunoprecipitation experiments demonstrated that quercetin did not disrupt physical interaction of phospho-Smad3 and Smad4 induced by TGF-β in 3T3 cells. Panel B: Similarly, quercetin treatment did not appear to disrupt TGF-β-induced translocation of the phosphoSMAD3 (green)/Smad4 (red) complex to the nucleus (blue) of NIH 3T3 cells. Panel C: Activity of a TGF-β-induced, Smad3/4-regulated transcriptional reporter system was not significantly altered by exposure to quercetin. Reporter activity is expressed as fold-induction of the secreted alkaline phosphatase as compared to dual vehicle (PBS + 0.1% DMSO) treated controls. Columns: mean of three independently replicated experiments, bars: SEM, brackets; $P < 0.05$ by ANOVA.

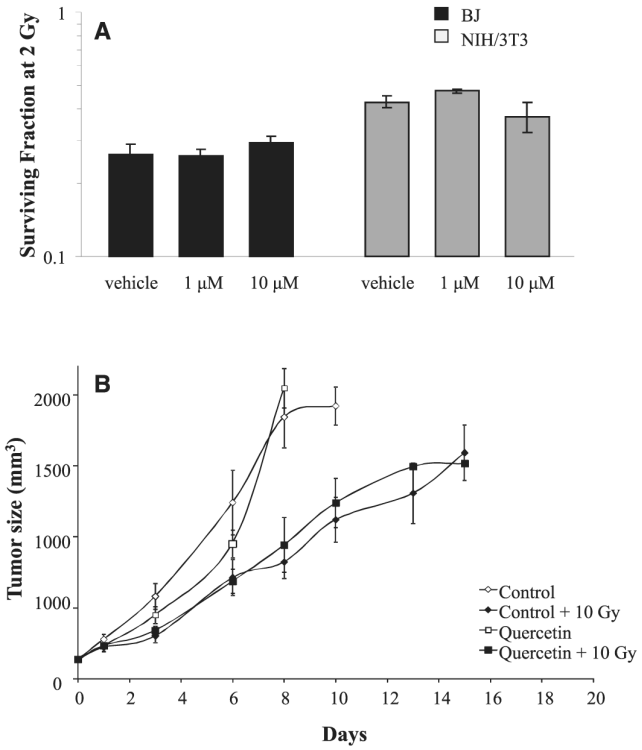

FIG. 5.

The effects of quercetin on radiation response. Panel A: Quercetin pretreatment did not offer a radioprotective benefit to mouse (NIH/3T3) of human (BJ) fibroblasts. Data shown are average clonogenic survival ±SEM in three independent experiments. Panel B: Quercetin treatment did not alter tumor radioresponse in mice bearing subcutaneous SCC-VII tumors. Data shown are mean tumor volume ±SEM.

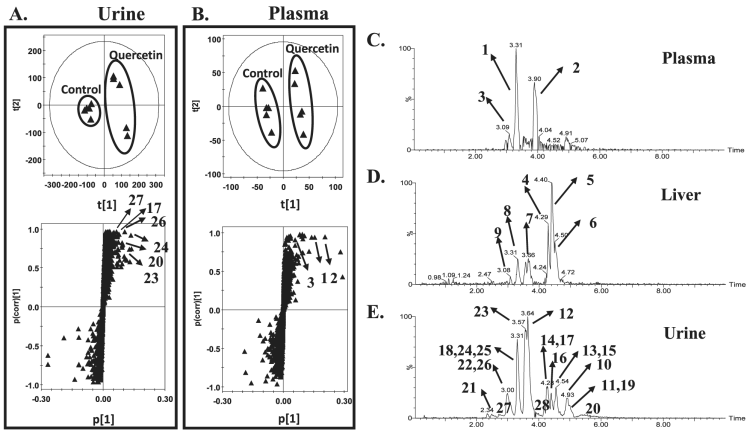

FIG. 6.

Identification of quercetin metabolites in urine, plasma, and liver using UPLC–ESI–QTOFMS based-metabolomics. Panel A: Scores plot of a PLS-DA model and OPLS loadings S-plot of urinary ions from control and quercetin-treated mice. Each point represents an individual mouse urine sample (top panel) and a urinary ion (bottom panel). Quercetin and its metabolites are labeled in the S-plot. Panel B: Scores plot of a PLS-DA model and OPLS loadings S-plot of plasma ions from control and quercetin-treated mice. Each point represents an individual mouse plasma sample (top panel) and a plasma ion (bottom panel). Quercetin and its metabolites are labeled in the S-plot. Panels C–E: Representative chromatograms of major quercetin metabolites in plasma, liver and urine samples of quercetin-treated mice. The code of metabolites is the same as the number in the Table 1.

TABLE 1

Quercetin Metabolites in Plasma Liver and Urine

No.	Retention time (min)	Observed *m/z*	Formula	Mass error (ppm)	Identity
Plasma					
1	3.31	653.099	C27H26O19[H-]	0.2	Quercetin diglucuronide
2	3.91	395.007	C16H12O10S[H-]	−0.2	Methylquercetin sulfate
3	3.09	667.118	C28H28O19[H-]	4.9	Methylquercetin diglucuronide
Liver					
4	4.29	491.081	C22H20O13[H-]	−2.4	Methylquercetin glucuronide
5	4.41	491.085	C22H20O13[H-]	5.5	Methylquercetin glucuronide
6	4.56	491.083	C22H20O13[H-]	1.8	Methylquercetin glucuronide
7	3.67	477.064	C21H18O13[H-]	−5.8	Quercetin glucuronide
8	3.32	653.099	C27H26O19[H-]	0.5	Quercetin diglucuronide
9	3.13	667.114	C28H28O19[H-]	−0.4	Methylquercetin diglucuronide
Urine					
10	4.93	301.042	C15H10O7[H-]	23.9	Quercetin
11	5.00	380.992	C15H10O10S[H-]	1.0	Quercetin sulfate
12	3.71	477.068	C21H18O13[H-]	2.3	Quercetin-3-glucuronide
13	4.58	477.073	C21H18O13[H-]	12.7	Quercetin-3′-glucuronide
14	4.31	477.067	C21H18O13[H-]	0.2	Quercetin-4′-glucuronide
15	4.61	491.082	C22H20O13[H-]	−1.2	Isorhamnetin-3-gluruonide
16	4.48	491.082	C22H20O13[H-]	−1.2	Isorhamnetin-7-gluruonide
17	4.33	491.085	C22H20O13[H-]	4.9	Isorhamnetin-4′-gluruonide
18	3.42	477.064	C21H18O13[H-]	−6.1	Isorhamnetin-3-glucuroside
19	4.98	557.023	C21H18O16S[H-]	−1.2	Quercetin glucuronide sulfate
20	5.38	557.025	C21H18O16S[H-]	2.3	Quercetin glucuronide sulfate
21	2.41	653.099	C27H26O19[H-]	0.0	Quercetin diglucuronide
22	3.06	653.097	C27H26O19[H-]	−3.1	Quercetin diglucuronide
23	3.68	653.101	C27H26O19[H-]	3.1	Quercetin diglucuronide
24	3.37	653.114	C27H26O19[H-]	22.9	Quercetin diglucuronide
25	3.34	667.114	C28H28O19[H-]	−1.0	Methylquercetin diglucuronide
26	3.14	667.115	C28H28O19[H-]	0.4	Methylquercetin diglucuronide
27	2.88	667.118	C28H28O19[H-]	4.9	Methylquercetin diglucuronide
28	4.01	667.118	C28H28O19[H-]	4.9	Methylquercetin diglucuronide